JOURNAL OF VIROLOGY, Apr. 2010, p. 3431–3442 Vol. 84, No. 7
0022-538X/10/$12.00 doi:10.1128/JVI.01735-09

Simian Virus 40 Infection Triggers a Balanced Network That Includes Apoptotic, Survival, and Stress Pathways▽†

Veronika Butin-Israeli,‡ Nir Drayman, and Ariella Oppenheim*

Department of Hematology, Hebrew University—Hadassah Medical School, Jerusalem, Israel 91120

Received 18 August 2009/Accepted 12 January 2010

The infection process by simian virus 40 (SV40) and entry of its genome into nondividing cells are only partly understood. Infection begins by binding to GM1 receptors at the cell surface, cellular entry via caveolar invaginations, and trafficking to the endoplasmic reticulum, where the virus disassembles. To gain a deeper insight into the contribution of host functions to this process, we studied cellular signaling elicited by the infecting virus. Signaling proteins were detected by Western blotting and immunofluorescence staining. The study was assisted by a preliminary proteomic screen. The contribution of signaling proteins to the infection process was evaluated using specific inhibitors. We found that CV-1 cells respond to SV40 infection by activating poly(ADP-ribose) polymerase 1 (PARP-1)-mediated apoptotic signaling, which is arrested by the Akt-1 survival pathway and stress response. A single key regulator orchestrating the three pathways is phospholipase C-gamma (PLCγ). The counteracting apoptotic and survival pathways are robustly balanced as the infected cells neither undergo apoptosis nor proliferate. Surprisingly, we have found that the apoptotic pathway, including activation of PARP-1 and caspases, is absolutely required for the infection to proceed. Thus, SV40 hijacks the host defense to promote its infection. Activities of PLCγ and Akt-1 are also required, and their inhibition abrogates the infection. Notably, this signaling network is activated hours before T antigen is expressed. Experiments with recombinant empty capsids, devoid of DNA, indicated that the major capsid protein VP1 alone triggers this early signaling network. The emerging robust signaling network reflects a delicate evolutionary balance between attack and defense in the host-virus relationship.

Viruses, the ultimate parasites, usurp cellular machinery for their life cycle. For this reason they have been instrumental in investigating basic genetic processes, including DNA replication, transcription, RNA processing, and translation. More recently, studies on virus-cell recognition and entry pathways revealed a wide spectrum of receptors, trafficking routes, and cellular signaling elicited by infecting viruses (43, 53, 64).

Cells commonly respond to pathogen infection by apoptosis, generally viewed as an "altruistic" measure taken by infected cells to save the population. During coevolution of host and pathogens, viruses have developed countermeasures to prevent or delay apoptosis until their propagation is accomplished (25). For example, viruses recruit DNA damage signaling to reprogram the cell for viral replication (35) and manipulate the host cell cycle response (61). Other mechanisms include inhibition of caspases (8) and expression of viral analogs of the apoptosis regulators of the Bcl-2 family (45).

The abundant nuclear enzyme poly(ADP-ribose) polymerase 1 (PARP-1) is a central player in DNA damage surveillance and repair, functioning at the decision between cell-cycle arrest, apoptosis, and necrosis (reviewed in reference 30). This 116-kDa protein is activated by binding to breakage points in the DNA and functions by catalyzing the addition of extensive, branched polymers of poly(ADP-ribose) (PAR) onto proteins, using NAD^+ as a substrate. Its activity is readily detected by ADP-ribosylation of nuclear proteins, in particular, transcription factors and chromatin modulators. PARP-1 is most active in automodification, and active PARP-1 is identified as an ADP-ribosylated species. It was shown to participate in maintaining genome stability and chromatin modulation. Active PARP-1 recruits DNA repair factors to the damaged DNA, leading to cell survival. On the other hand, unregulated activation of PARP-1 may lead, through NAD^+ utilization, to energy depletion and subsequent cell necrosis. Necrotic cell death may be prevented by activation of caspases, which cleave PARP-1 and direct the cell to apoptosis (30).

Caspase activation occurs through two main apoptotic pathways, intrinsic and extrinsic. In the intrinsic pathway caspases are activated from the mitochondria in response to cellular signals resulting from severe cell stress, such as DNA damage, defective cell cycle, hypoxia, and loss of cell survival factors (reviewed in reference 24). Most of the signals are mediated by p53 and lead to activation of initiator caspase-9, followed by formation of the apoptosome with cytochrome *c* and Apaf-1 (34). This leads to activation of an expanding cascade of caspase-3, -6, and -7 that carry out apoptosis.

Caspases may also be activated by external signals via ligand-specific activation of proapoptotic receptors (death receptors) on the cell surface, including members of the tumor necrosis factor (TNF) family receptors and others (reviewed in references 5 and 56). This extrinsic apoptotic pathway is mostly p53 independent. The external death signal is mediated by death receptor clustering, recruitment of the adaptor proteins with the Fas-associated death domain (FADD), and an activation of initiator caspase-8 or -10, forming a death-inducing signaling

* Corresponding author. Mailing address: Department of Hematology, Hebrew University—Hadassah Medical School, Jerusalem, Israel 91120. Phone: 972 2 6776753. Fax: 972 2 6423067. E-mail: ariella.oppenheim@mail.huji.ac.il.

‡ Present address: Department of Cell and Molecular Biology, Feinberg School of Medicine, Northwestern University, Evanston, IL.

† Supplemental material for this article may be found at http://jvi.asm.org/.

▽ Published ahead of print on 20 January 2010.

complex (DISC) (reviewed in references 5 and 56). Usually, caspase-3, -7, and -6 are active during the progress of both the typical intrinsic and the extrinsic apoptotic pathways (11).

Another major player in the decision between cellular life and death is Akt-1, a downstream target of phosphatidylinositol 3-kinase (PI3K) (14, 21). Akt-1 is a Ser/Thr kinase, fully activated by phosphorylation at S473. Akt-1 functions as an antiapoptotic signaling protein by activating the survival pathway. This is achieved by inhibition (via phosphorylation) of caspase-9 and Apaf-1 as well as other proapoptotic proteins such as BAD and its downstream target BAX (36). Active Akt-1 commonly leads to cell proliferation and plays a role as an oncogene in tumorigenic processes (6, 52).

In addition to Akt-1, chaperones, whose major role is in protein quality control, also function in cell rescue and survival (4, 7). Heat-induced as well as constitutive chaperones interact with members of apoptotic signaling pathway at multiple levels. Thus, chaperones may limit the apoptotic cascade and facilitate cell recovery.

Phosphoinositide-specific phospholipase C-gamma (PLCγ) catalyzes the hydrolysis of phosphoinositides into the second messengers inositol 1,4,5-triphosphate (IP3) and diacylglycerol (DAG). PLCγ is activated via phosphorylation by activated protein tyrosine kinase receptors. It is subsequently released and functions, through additional partners, in simultaneous activation of divergent pathways, including production of PI(3,4,5)P3, generation of IP3, elevation of cytoplasmic calcium, and activation of Ras/Raf/MEK/mitogen-activated protein kinase (MAPK) and other protein kinase cascades (42).

Simian virus 40 (SV40), a nonenveloped primate virus, is a member of the *Polyomaviridae* family and a close relative of the human pathogens BK virus and JC virus. The capsid is composed of three virus-encoded proteins: the major protein VP1 and the two minor proteins VP2 and VP3. Seventy-two identical pentamers of VP1 form the icosahedral capsid, while VP2 and VP3 bridge between the outer shell and the chromatin core (55).

Many viruses enter the host cell via organelles involved in clathrin-dependent endocytosis. They are transported to early and late endosomes, where they undergo partial or complete disassembly in moderately acidic pH (reviewed in references 37 and 53). In contrast, SV40 and other polyomaviruses, which infect nondividing cells, enter host cells by an atypical clathrin-independent endocytic process mediated by caveolae, which are caveolin-1-containing flask-shaped invaginations in lipid rafts (3, 20, 46, 54), and undergo disassembly in the endoplasmic reticulum (ER) (40). SV40 cell entry begins with viral binding to its receptor, GM1 ganglioside (13, 57). The structure of VP1 complexed with the carbohydrate portion of GM1 has been recently resolved (39). Binding of SV40 to its receptor induces membrane invaginations in an energy-independent process (22).

The SV40 infection process is slow. At 5 to 6 h postinfection VP2/VP3 (VP2/3) becomes detectable in the ER as a consequence of SV40 conformational changes and/or disassembly facilitated by ER chaperones (40, 51). It was recently demonstrated that chaperones participate in SV40 disassembly *in vitro* (17). Viral DNA is first seen in the nucleus of CV-1 cells only after 8 h of infection (IKopatz and A. Oppenheim, unpublished data), as determined by analysis of SV40 DNA (by quantitative PCR) in nuclei isolated from infected cells. The mechanism by which the DNA enters the nucleus in nondividing cells is poorly understood.

SV40 triggers kinase-dependent signals that promote dynamin recruitment and actin disassembly and repolymerization (44). In addition, both polyomavirus and SV40 were found to activate the ATM DNA damage response pathway following their entry and T-antigen expression, presumably to enhance viral DNA replication (18) (62).

To obtain an insight into mechanisms that facilitate nuclear entry of the viral genome, we focused in the present study on early cellular signaling elicited by the virus prior to nuclear entry and T-antigen expression. Thus, signals induced by the viral T antigen were excluded. We have found a unique combination of proapoptotic, cell survival, and stress response signaling.

MATERIALS AND METHODS

Antibodies. The following antibodies were used: Akt-1, polyclonal; phospho-Akt-1 (P-Akt-1), polyclonal against phosphorylated S473; P-Bad, polyclonal; caspase-9, monoclonal; caspase-9, polyclonal; P-caspase-9, polyclonal; caspase-3, polyclonal; cleaved caspase-3, polyclonal; caspase-7, polyclonal; and P-PLCγ polyclonal antibodies (Cell Signaling). Polyclonal caspase-6 antibodies were from Cell Signaling, Santa-Cruz, and Abcam. Hsp70/Hsc70 (Hsp/c70) monoclonal antibody (clone BB70; Stressgen) was used. Other antibodies were as follows: anti-PAR, polyclonal; PARP-1, rabbit polyclonal (Alexis) and rabbit and goat polyclonal (Santa-Cruz); SV40 T antigen, monoclonal; caspase-10, polyclonal; caspase-8, polyclonal; lamin B, polyclonal; emerin, polyclonal antibodies (Santa Cruz). VP1 and VP2/3 polyclonal antibodies were prepared in our laboratory (50). For confocal microscopy we used Cy2-, Cy3-, and Cy5-conjugated secondary antibodies (Jackson).

Inhibitors. The following inhibitors were used: PI3K inhibitor LY294002 (Cell signaling), PLCγ inhibitor U73122, Akt inhibitor Tricibine V (Calbiochem), pan-caspase inhibitor Z-VAD-FMK (where FMK is fluoromethyl ketone), caspase-6 inhibitor Ac-VEID-CHO (where Ac is acetyl and CHO is aldehyde), caspase-10 inhibitor Z-AEVD-FMK, and caspase-3 inhibitor Ac-DMQD-CHO (Alexis). Note that Ac-VEID-CHO and Z-AEVD-FMK overlap in inhibition of both caspase-6 and -10 (and also caspase-8).

Inhibitors were used at nontoxic levels, as determined by preliminary assays. Inhibitors were added to the cells 1 h before adsorption, and the inhibitor-containing medium was removed before the infection began. Infection was carried out as described below.

Cell cultures. CV-1 (ATCC CCL70) are African Green monkey cells. PARP-$1^{-/-}$ (clone A12) and PARP-$1^{+/+}$ (clone A19), derived from murine PARP-1 knockout mouse (58), were generously provided by Z. Q. Wang. Cells were cultured in high-glucose Dulbecco's modified Eagle's medium (DMEM) containing glutamine, penicillin, streptomycin, and 10% fetal bovine serum (FBS). *Spodoptera frugiperda* (Sf9) cells were grown at 27°C in serum-free Bio-insect medium containing glutamine, penicillin, streptomycin, and amphotericin.

SV40 production and purification. SV40 was propagated on CV-1 cells. Cells were harvested on the fifth day postinfection by the didetergent method (48). Triton X-100 and deoxycholate were added to the culture medium to final concentrations of 1% and 0.5%, respectively. The cell suspension was centrifuged at 9,500 rpm (10,000 × *g*) for 30 min at 4°C to precipitate debris. The virus was sedimented by centrifugation at 80,000 × *g* for 4 h at 4°C. The viral pellet was resuspended in phosphate-buffered saline (PBS) overnight at 4°C, sonicated, and centrifuged to clarify the virus suspension. Titration was performed by scoring for replication centers in CV-1 cells infected at different dilutions. Replication centers were scored at 2 days postinfection at the peak of viral DNA replication by *in situ* hybridization with SV40 DNA labeled with [α-^{32}P]dCTP.

Production and purification of VLPs. Recombinant baculovirus expressing VP1 (SwissProt P03087; PDB 1SVA) from the polyhedrin promoter was used for production of virus-like particles (VLPs) as previously described (50). The VLPs were harvested from the medium of baculovirus-infected Sf9 cells following cell lysis at 5 days postinfection as follows: intact cells and cell debris were removed by centrifugations at 6,000 × *g* for 10 min. The supernatant was further clarified at 17,000 × *g* for 20 min. VLPs were precipitated at 80,000 × *g* for 3 h. The VLP pellet was suspended in 0.5 M NaCl, purified by ultrafiltration, and stored at −20°.

SV40 and VLP infection experiments. SV40 was added to confluent CV-1 monolayers at a multiplicity of infection (MOI) of 10 in a small volume of

serum-free medium and grown in 10-cm-diameter tissue culture dishes. Alternatively, 50 ng of VLPs was added per 10^6 cells, approximately equivalent to an MOI of 10 capsids per cell. (The molecular mass of a VP1 capsid is ~15 MDa, and thus 50 ng represents $\sim 2 \times 10^9$ capsids; as ~1 in 200 particles in SV40 stocks is infectious [10; also our unpublished data], 2×10^9 SV40 virions contain 1×10^7 infectious particles, or an MOI of 10 when applied to 10^6 cells.) Confluent CV-1 monolayers were washed twice with PBS. To synchronize the infection, the virus or VLPs were allowed to adsorb to the cells for 40 min at 4°C on a gyratory shaker at 20 rpm. Nonadsorbed virus or VLPs were washed twice with serum-free medium (SFM), followed by addition of DMEM–10% fetal calf serum (FCS), and the cells were transferred to 37°C until harvest. This point was considered time zero.

Proteomics screen. We used a Hypromatrix signal transduction antibody array and phosphorylated serine (P-Ser) horseradish peroxidase (HRP)-conjugated antibody. The procedure was based on the manufacturer's protocol (Hypromatrix) with some modifications. Briefly, the soluble fractions of SV40-infected cell lysates were incubated with the array overnight at 4°C, washed, incubated with the detection antibody for 4 h at 4°C, and washed, and enhanced chemiluminescence (ECL) analysis was performed according to standard practice using Pierce ECL Western blotting substrate. Phosphorylation intensity was quantified using densitometry, and data were exported to Excel for further analysis, including background subtraction, present/absent determination, normalization, and flooring and filtering out of unchanged proteins. Clustering was preformed using MeV software, and annotation was done using the DAVID website.

Protein analyses. Total cell lysates were prepared by lysis in a solution containing 0.6% SDS–10 mM Tris (pH 7.4) and boiling for 10 min. Samples containing 20 μg of protein were loaded on each lane. Cytoplasmic and nuclear fractions were separated by centrifugation following treatment with 10% NP-40. Nuclear extracts were prepared as previously described (50). Polyacrylamide gel electrophoresis (PAGE) and Western blot analyses were performed using NuPAGE 4 to 12% Bis-Tris gels (Invitrogen), transferred to Immobilon membranes (Millipore), and detected with appropriate antibodies.

Immunoprecipitation. Two hundred micrograms of total cell lysates was diluted with immunoprecipitation buffer (50 mM Tris, pH 7.4, 2 mM EDTA, 2 mM EGTA, 1 mM dithiothreitol [DTT], 1 mM phenylmethylsulfonyl fluoride [PMSF], and complete protease inhibitors [Roche]) to a final volume of 0.5 ml. The samples were incubated for 1 h at 4°C with protein A/G agarose beads (Santa Cruz) for preclearing, followed by incubation with the primary antibody overnight at 4°C with agitation. In the next steps protein A/G agarose beads were added and incubated with the antigen-antibody complex for 1 h at 4°C. Following immunoprecipitation, the pellet was washed once with 0.5% SDS solution and twice with 0.5% Tween-20 solution. The immunoprecipitated proteins were eluted in a small volume of Laemmli loading buffer and boiled for 10 min.

TUNEL detection. DNA strands breaks were detected by terminal deoxynucleotidyltransferase-mediated dUTP-biotin nick end labeling (TUNEL), using an *in situ* cell death detection kit and fluorescein (Roche), according to the manufacturer's protocol. Briefly, the cells were fixed with 4% formaldehyde, followed by permeabilization by Triton X-100, labeling with terminal transferase, and detection by fluorescence microscopy. Negative-control slides were incubated with the same labeling solution without terminal transferase. Positive-control slides were prepared by adding DNase I (5 μg/ml) for 1 h at room temperature after permeabilization. Images were taken under a fluorescent microscope.

Immunostaining. Confluent CV-1 cells grown on coverslips and infected with SV40 or VLPs were fixed in 4% formaldehyde for 15 min at room temperature and permeabilized by treatment with 0.5% Triton X-100 for 10 min. The cells were incubated with the appropriate antibody for 18 h at 4°C. Staining with secondary antibody conjugated to Cy2 or Cy5 was done for 1 h at room temperature. Analyses were performed by confocal microscopy (Zeiss). Differential interference contrast (DIC) imaging, according to Nomarski, was used in order to define the nucleus. To ascertain that confocal images were collected on similar planes, *Z*-sectioning was performed before images were taken.

RESULTS

Activation of PARP-1. To obtain an overview of signaling pathways elicited by the infecting virus, we performed a proteomic screen using Hypromatrix signal transduction arrays containing 400 antibodies (see Fig. S1 and S2 in the supplemental material). The three main pathways induced within 1 h postinfection were apoptosis (51 proteins), antiapoptosis (35 proteins), and DNA damage response (29 proteins). We were struck by the early activation of the DNA damage response, in particular, signals for DNA repair (BRCA1, BRCA2, Rad, Nibrin, and others), since it is highly unlikely that SV40 induces DNA breakage before its genome enters the nucleus and starts transcribing (see Fig. 3 below for evidence that there is no DNA damage at that time). We therefore searched for a candidate protein that could activate this unexpected signaling.

PARP-1 is activated by automodification by the addition of poly(ADP-ribose) chains. Thus, activated PARP-1 may be significantly larger than nonactive PARP-1 and readily distinguishable on protein gels. We tested for PARP-1 activation following infection of primate CV-1 cells at a multiplicity of 10 PFU per cell to ensure that most of the cells were infected. To avoid background signaling of cell cycle regulators, we infected confluent monolayers, mostly arrested in G_1 (see below and Fig. 5A). Viral adsorption was performed at 4°C in the absence of serum in order to synchronize the infection, which started with the addition of serum-containing medium and transfer to 37°C. Mock-infected cells were similarly treated, including cold incubation in the absence of serum, but without virus. This infection protocol was used throughout the study. We did not observe any temporal variations in the mock-infected cells; therefore, only a single time point of mock infection is presented in the figures. All the experiments were reproduced in at least two to three independent infection experiments (some were reproduced in five or six experiments and more) using different virus batches.

We were surprised to see extensive activity of PARP-1 starting at 1 h postinfection in total cell and nuclear extracts. The experiments were done by Western blotting with antibodies against poly(ADP-ribose) chains (anti-PAR). Direct evidence for PARP-1 activation was obtained by identifying poly(ADP-ribosylated) PARP-1 as follows: PARP-1 was immunoprecipitated from cellular extracts with anti-PARP-1 antibody, followed by Western blotting and detection with anti-PAR antibody (Fig. 1A). The data were highly reproducible using different antibodies as well as reverse immunoprecipitation (data not shown). The results showed that PARP-1 itself is poly(ADP-ribosylated) already at 1 h postinfection. The molecular mass of PARP-1 is 116 kDa (Fig. 1A, mock). The larger, poly(ADP-ribosylated) derivative of PARP-1 was seen by 1 h postinfection. In addition, the protein level of PARP-1 was elevated, with a peak at 4 to 6 h (Fig. 1F; see also Fig. 6B where the average of three independent experiments is shown). These experiments indicate that PARP-1 is activated very early in the infection cycle and remains active during the first 8 h.

PARP-1 activation could be an irrelevant corollary of SV40 infection. Alternatively, it could represent a necessary signal facilitating the infection. Small interfering RNA (siRNA) is a powerful method to test for the necessity of cellular proteins. However, in preliminary experiments we have observed that application of siRNA technology to our system is problematic since in the G_1-arrested cells that we have been using, transcription and protein synthesis are highly reduced. Therefore, to investigate whether PARP activity is required for the infection, we have used a murine PARP-1 knockout cell line (58) (kindly provided by Z. Q. Wang) and its wild-type parent as a control. Productive SV40 infection was assayed by detection of the viral early gene product, T antigen, at 48 h. Figure 1B

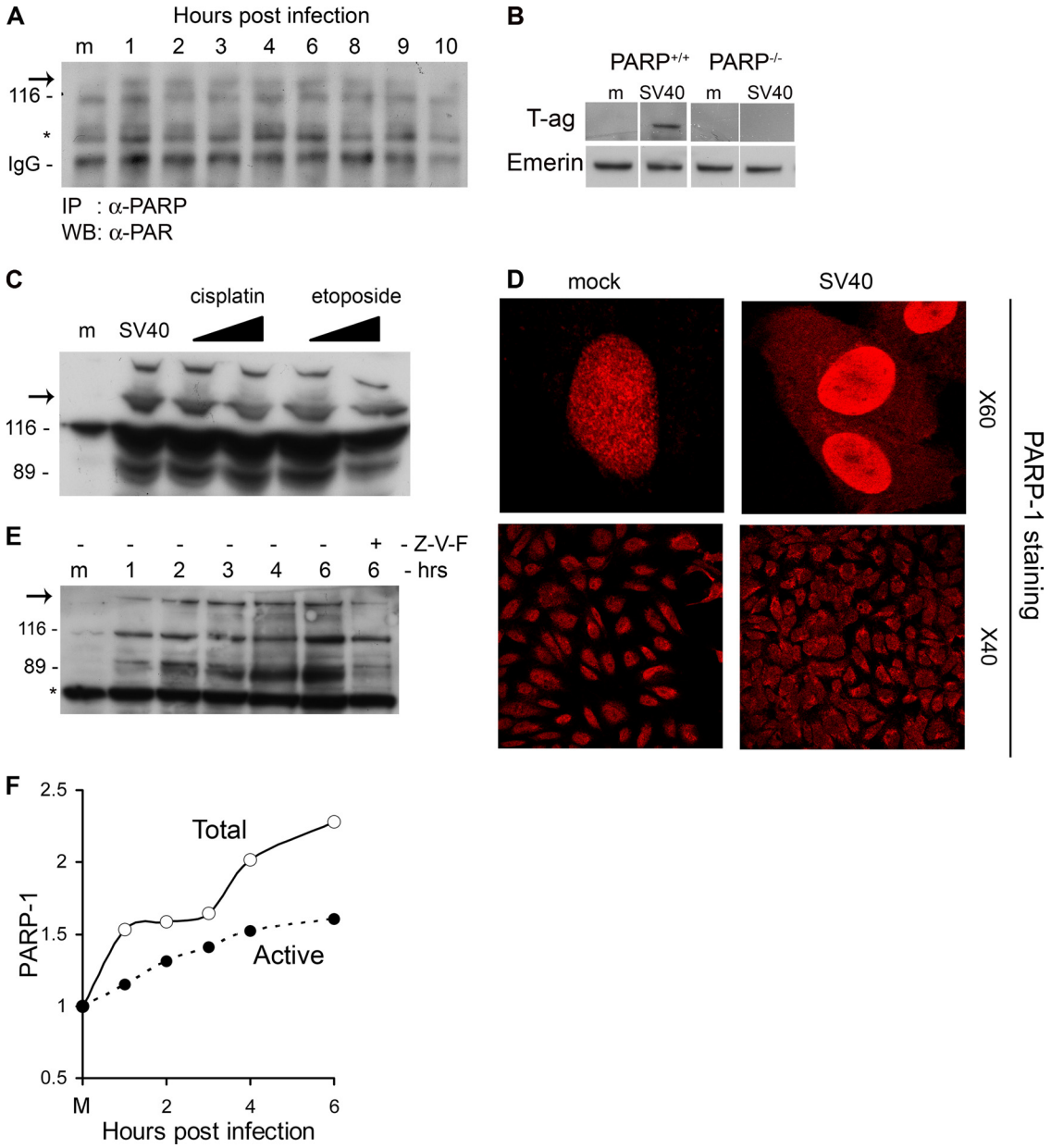

FIG. 1. Activation of PARP-1 and Caspases. (A) PARP-1 was immunoprecipitated from total cell extracts at the designated time points with anti-PARP-1 antibodies. Western detection was performed with anti-PAR antibody. PARP-1 is 116 kDa. The arrow points to active, poly(ADP-ribosylated) PARP-1. IgG served as a loading control. (B) PARP-1 is required for the infection to proceed. $PARP^{+/+}$ and $PARP^{-/-}$ cell lines were assayed for T-antigen expression 48 h after infection. Nuclear extracts were prepared, and T antigen was analyzed by Western blotting. Emerin detection served as a loading control. In this experiment we used an exceptionally high MOI of 500 because mouse cells are nonpermissive for productive SV40 infection as they do not support T-antigen-dependent viral DNA replication (9). (C) Cleavage by caspases. The Western blot shows the uncleaved 116-kDa protein and the 89-kDa caspase cleavage product. Etoposide and cisplatin were added at 15 and 30 μM. Western blotting was performed 48 h after the addition of etoposide and cisplatin and 6 h after infection by SV40. The arrow indicates active, poly(ADP-ribosylated) PARP-1. (D) Cellular distribution of PARP-1. Cells were fixed with 4% formaldehyde at 6 h postinfection and stained with polyclonal anti-PARP-1 and Cy3. Images in the top panels were taken at magnification of ×60 with zoom 3; lower images are at a magnification of ×40. Control and infected cells were at the same confluence. (E) Detection of active PARP-1 in total cell lysates. Western blotting was performed following loading of 20 μg of total protein per lane. The arrow points to higher-molecular-weight species of PARP-1 with extensive poly(ADP-ribosylation). The 89-kDa caspase cleavage product is significantly reduced in the presence of a 70 μM concentration of the pan-caspase inhibitor Z-VAD-FMK (Z-V-F). This experiment was reproduced five times. (F) Quantification of PARP-1 and active poly(ADP-ribosylated) PARP-1 following SV40 infection.

demonstrates that the level of T antigen in the $PARP^{-/-}$ cells is significantly lower than that in the $PARP^{+/+}$ cells, suggesting that PARP-1 plays a role in SV40 infection.

The dominant outcome of high PARP-1 activation is necrosis due to depletion of NAD^+ and ATP. Moderately activated PARP-1 leads to apoptosis. Activated caspase-3, -7, and -6 cleave PARP-1 into inactive 89-kDa and 24-kDa derivatives. The 89-kDa cleavage product is commonly used as a hallmark

of apoptosis (31). Western analysis of PARP-1 in 6-h-infected CV-1 cells showed the appearance of the activated PARP-1 and an 89-kDa band (Fig. 1C), reflecting caspase activities. This experiment also shows that the level of PARP-1 is increased postinfection.

As positive controls for PARP-1 activation and cleavage, we used CV-1 cells treated with known apoptotic triggers, etoposide (15 and 30 μM) and cisplatin (15 and 30 μM). As expected, both apoptotic reagents (at both concentrations) triggered PARP-1 activation and caspase cleavage (Fig. 1C) and caused ~50% cell death in 48 h and >95% in 80 h, as measured by trypan blue staining, in four independent experiments. Figure 1C shows that PARP-1 activation and cleavage patterns in SV40-infected cells at 6 h postinfection are essentially the same as those seen at 48 h following treatment by etoposide and cisplatin.

Additional evidence for the cleavage of PARP-1 comes from confocal microscopy (Fig. 1D, top panels). As expected, in the mock-infected cells PARP staining is exclusively nuclear. As the 89-kDa PARP-1 cleavage product does not contain the DNA-binding domain, it typically relocates from the nucleus to the cytoplasm. Indeed, Fig. 1D shows positive staining with anti-PARP antibody in the cytosol of the SV40-infected cells at 6 h postinfection. Note that PARP-1 staining is significantly more intense in the SV40-infected cells (stained and photographed under identical conditions to mock-infected cells), reflecting the increase in the level of PARP-1.

The bottom panels of Fig. 1D demonstrate that both activation and cleavage of PARP-1 are not sporadic and occur throughout the infected culture. The mock-infected cells show exclusively nuclear staining while in the virus-infected cells there is also extensive staining in the cytoplasm. This indicates that this proapoptotic signaling is a general outcome of the infection and does not occur preferentially in a subclass of the culture. Similar pictures were obtained in a number of independent experiments using three different anti-PARP antibodies. Control staining for VP1 indicated that essentially all the cells were infected (see Fig. S3A in the supplemental material).

To determine whether the cleavage is caspase dependent, the pan-caspase inhibitor Z-VAD-FMK (Fig. 1E, Z-V-F) was added to the cells 1 h prior to virus adsorption. Figure 1E shows that PARP-1 cleavage was significantly reduced. These results taken together indicate that (i) the PARP-1 level is increased postinfection (Fig. 1C, D, E, and F), (ii) PARP-1 is activated within 1 h following SV40 infection and remains active for at least 8 h (Fig. 1A, E, and F), and (iii) PARP-1 is cleaved by caspases, as in a classical apoptotic pathway (Fig. 1C, D, and E).

Caspases participate in SV40 infection. Our next step was to determine which caspases function in PARP cleavage following infection. PARP-1 is typically cleaved by caspase-3 or -7 and may also be cleaved by caspase-6. Caspases are activated by proteolytic cleavage, detectable by Western blotting. The results (Fig. 2A, left panel) show a very low level of the active form of caspase-3. The same results were seen using an antibody specific for the cleaved form of caspase-3 (data not shown). Note that caspase-3 is activated only at 5 to 6 h and therefore cannot be implicated in PARP-1 cleavage at 1 h (Fig. 1E and F). The second candidate, caspase-7 (Fig. 2A, right panel) does not appear to be activated following SV40 infection. On the other hand, the active form of caspase-6 is present at 1 to 8 h of infection, albeit at a very low level relative to its procaspase. This low-level activation, however, is highly reproducible: the experiment with caspase-6 was repeated many times, with three different antibodies from three different sources (see Materials and Methods). Positive control for caspase-6 activation is seen in Fig. 2B (right). The simplest explanation of these data, taken together, is that caspase-6 is responsible for PARP-1 cleavage following SV40 infection, as seen in Fig. 1C.

To unravel the pathway of caspase-6 activation, we tested for activation of the initiator caspases 9, 8, and 10. In repeated experiments we have never seen cleavage of initiator caspase-8 and -9 to their active forms (Fig. 2A, right panel). Caspase-9 was tested with two different antibodies. As shown below (see Fig. 4A), following infection caspase-9 is also inhibited via partial serine phosphorylation. On the other hand, the active form of caspase-10 is present from 1 h postinfection (and absent in mock-infected cells). There is also significant elevation in the level of procaspase-10 (Fig. 2A, left panel). Caspase-10 was previously reported to participate in activation of caspase-6 (41). Consistent with that study, inhibition of caspase-10 eliminated the appearance of active caspase-6 in our experiments (Fig. 2B).

In spite of the low level of caspase activation, general inhibition with a pan-caspase inhibitor and specific inhibition of caspase-10 and -6, but not caspase-3, completely blocked the infection, as assayed by T-antigen production (Fig. 2C). It appears that not every caspase that is activated following infection is required for the process to proceed. Control Western blotting for VP1 indicated that all the cultures were infected by SV40, including those that did not show T-antigen staining (see Fig. S3B in the supplemental material). Although the inhibitors are not absolutely specific (38), it appears that caspase-10 and -6 are obligatory participants in SV40 cell entry mechanism. One attractive explanation might be that cleavage of the capsid proteins occurs as part of the disassembly process. However, SV40 capsid proteins do not appear to be cleaved by caspases, as found for other viruses such as influenza virus (63), feline calicivirus (2), and Aleutian mink disease virus (16). Caspase cleavage sites were not identified by bioinformatics analysis, and cleavage of the capsid proteins was not detected by Western analysis, suggesting a different role for caspases in SV40 infection.

SV40-infected cells do not undergo apoptosis or DNA damage in the first 24 h. Cleavage of PARP-1 by caspases is a hallmark of apoptosis. We tested the infected cells by TUNEL staining, which detects DNA damage in apoptotic cells, from 9 to 24 h postinfection. The results for the infected cells were completely negative (Fig. 3, top panels) while both positive controls, CV-1 cells treated with etoposide (30 μM) or with DNase I, showed extensive staining (bottom panels). Furthermore, the SV40-infected cells were >95% alive and well, as measured by trypan blue staining. This indicates that in spite of the induction of proapoptotic signaling in all the infected cells (Fig. 1), there was no DNA damage or apoptotic cell death.

Supporting data were provided by flow cytometry of SV40-infected cells (see Fig. 5A): sub-G_1 peak, the cell cycle marker for apoptosis (33) was not detected in those experiments.

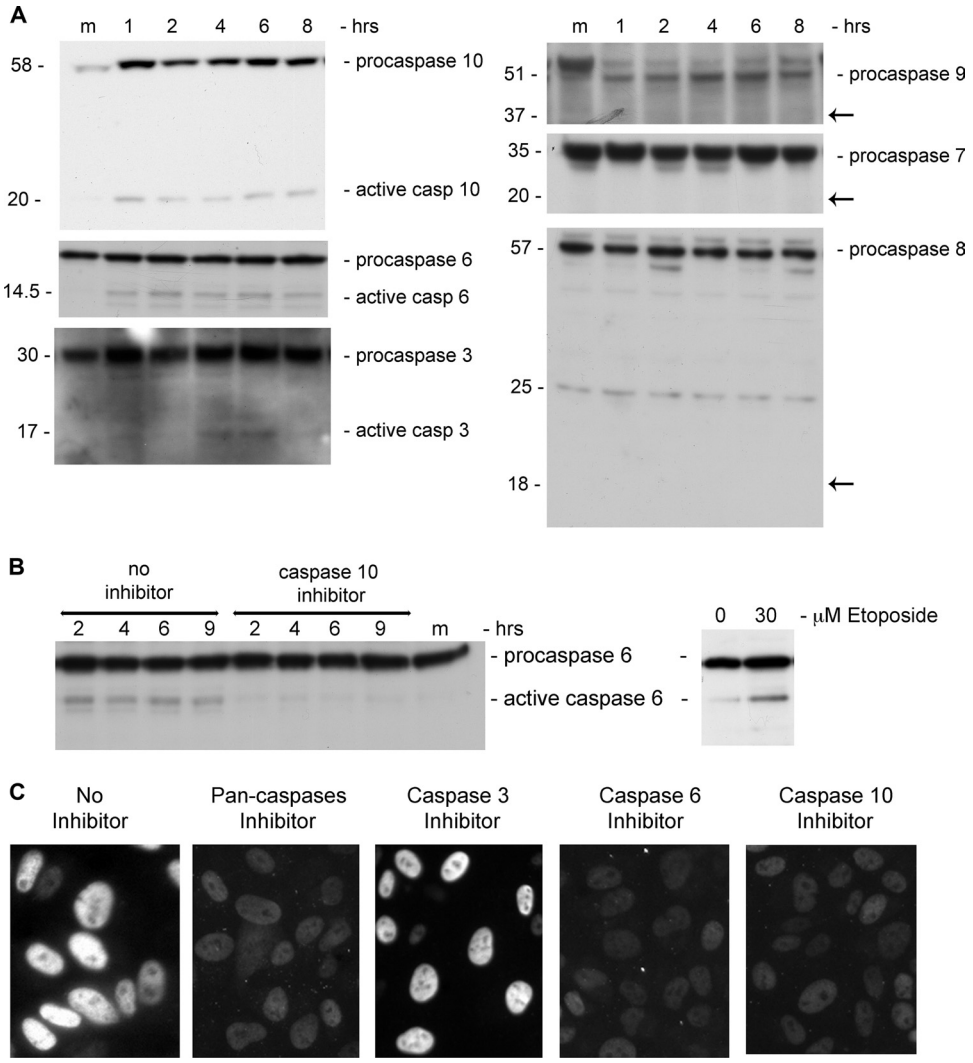

FIG. 2. Caspase activation. (A) The left panels show caspases that are activated following SV40 infection, as indicated by the cleavage products: 20-kDa fragment of caspase-10, 14.5-kDa fragment of caspase-6, and 17-kDa fragment of caspase-3. Arrows on the right panel point to the expected locations of cleavage products of caspase-9 (37 kDa), caspase-7 (20 kDa), and caspase-8 (18 kDa). (B) Activation of caspase-6 by caspase-10. Caspase-6 cleavage is inhibited following the addition of caspase-10 inhibitor (left). Positive control for caspase-6 activation by etoposide treatment (30 μM) is seen on the right. The cells were harvested 48 h after etoposide addition when ~50% were dead. (C) Expression of T antigen in infected CV-1 cells in the presence of the following inhibitors: all caspases, 70 μM Z-VAD-FMK; caspase-3, 20 μM Ac-DMQD-CHO; caspase-6, 20 μM aldehyde; caspase-10, 5 μM Z-AEVD-FMK. Images were obtained by fluorescence microscopy at a magnification of ×40.

Apoptotic arrest. Activation of PARP-1 and caspases in the absence of DNA damage and the lack of apoptosis were puzzling, indicating that additional signaling pathways were operating. To obtain a wider view of signals triggered by the infecting virus, we performed proteomic screening for serine phosphorylation using antibody arrays, as described in Materials and Methods. Hypromatrix signal transduction antibody array membranes were treated with cellular extracts, which was followed by detection with anti-phosphoserine antibodies. The left panels of Fig. S1 in the supplemental material show that the overall spot intensity increased substantially from the mock array to the 1- and 6-h arrays. Out of the 400 signaling proteins present on the array, 370 spots were positive in at least one membrane. Annotation of these proteins revealed that 183 of the phosphorylated proteins belong to apoptosis/survival pathways. Clustering of these proteins is shown in Fig. S1 (right panel). Phosphorylation of the Ser/Thr kinase Akt-1 was particularly dramatic: compared to the mock-infected cells there was a 10-fold increase at 1 h and a 26-fold increase at 6 h (Fig. S1, left panels, and S2, immediate response cluster). The data also showed phosphorylation of Akt-1's downstream substrates, caspase-9 and Apaf-1, as well as of other proapoptotic proteins, e.g., BAD and its downstream target BAX (36).

We therefore considered Akt-1 as a candidate player in activating survival pathway signaling. To validate the proteomics results, we performed independent Western analysis for P-Ser473 Akt-1, the fully active kinase. As seen in Fig. 4A (and quantified in Fig. 6B below), P-Akt-1 is hardly detected in the mock-infected cells while it is detected throughout the first 8 to 9 h of infection, with peaks at 2 and 5 to 6 h. Note that the level of the Akt-1

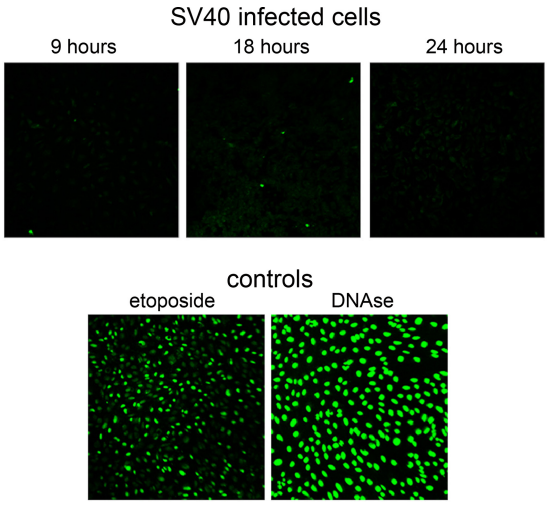

FIG. 3. SV40-infected cells do not undergo apoptosis or DNA damage during the first 24 h following infection. SV40-infected cells and controls were assayed by TUNEL staining. SV40-infected cells were assayed at the indicated time points. Etoposide-treated cells are shown at 48 h after addition. At that time ~75% of the cells were TUNEL positive, indicating DNA damage, and ~50% were dead, measured by trypan blue staining. DNase I-treated cells were photographed 1 h after Triton X-100 permeabilization.

protein is also increasing during early infection. Staining for P-Akt-1 in CV-1 cells at 6 h postinfection (Fig. 4B) demonstrates that, as seen above for PARP-1 (Fig. 1D), Akt-1 activation is also general, not sporadic. Figure S3C in the supplemental material shows that all cells were also positive for VP1.

Additional validation of the pathway was performed by testing for serine phosphorylation of two targets of Akt-1, BAD and caspase-9 (Fig. 4A). Both are active in the apoptotic pathway when they are nonphosphorylated and inhibited by Akt-1-mediated phosphorylation. Their temporal phosphorylation in our experiments is consistent with Akt-1 activity.

We conclude that Akt-1 is activated soon after SV40 infection, leading to induction of a survival pathway and to apoptotic arrest. Although the level of caspase-9 phosphorylation has been consistently low (Fig. 4A and a number of additional experiments), we have never seen activation of caspase-9 by cleavage of the procaspase (Fig. 2A, right panel). Inactivation by phosphorylation of BAD, BAX, and Apaf-1 (seen in the proteomics arrays Fig. S2 in the supplemental material) and the absence of cleaved caspase-9 are consistent with prevention of apoptosome formation.

We have used the Akt-1-specific inhibitor Tricibine V to test whether its activity is required for the infection. The addition of Tricibine completely abolished T-antigen expression in the infected cells (see Fig. 6C below), indicating that Akt-1 is playing a critical role in SV40 infection. The control experiment (see Fig. S3C in the supplemental material) shows that the cells were positive for VP1.

The stress response of the host to viral infection may also function in apoptotic arrest (7). In addition to Akt-1, Hsp70 was also implicated in inhibition of apoptosome formation via negative regulation of Apaf-1 (49). Our experiments show that following infection, Hsp/c70 is upregulated in two waves, with peaks at 2 and 6 h (Fig. 4C; quantified below in Fig. 6B). The second wave is higher than the first. Such a pattern of Hsp70

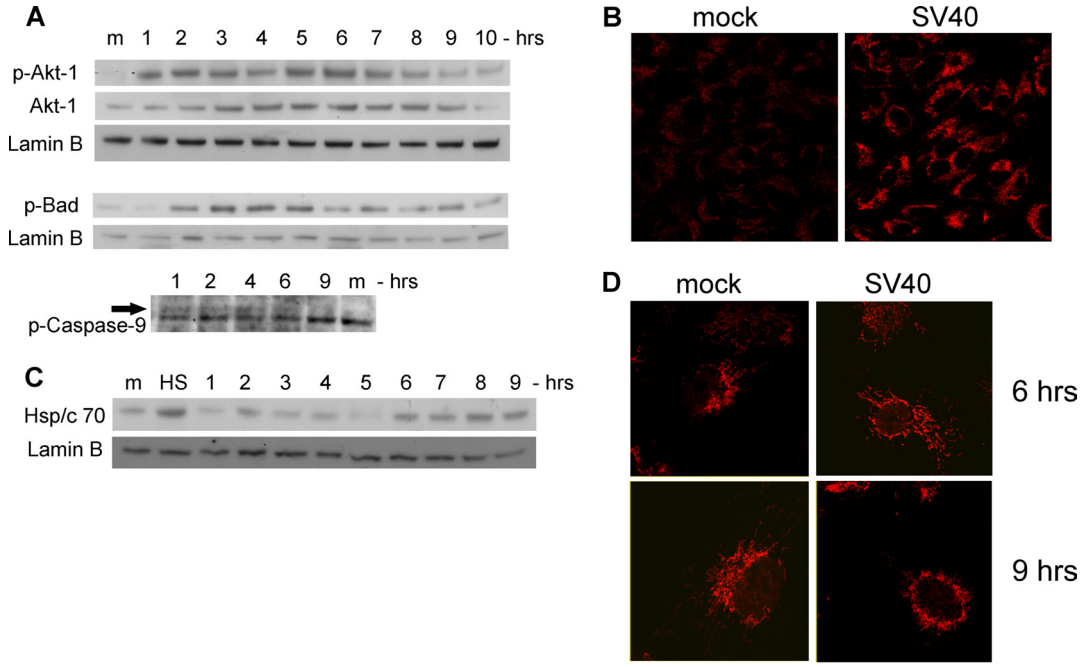

FIG. 4. Activation of survival pathway and stress response. (A) Western blotting showing activation of Akt-1 by phosphorylation (top), upregulation of Akt-1 protein (middle), and inhibition of BAD and caspase-9 by phosphorylation. Lamin B served as a loading control. (B) Detection of phospho-Akt-1 by immunostaining. Cells were fixed with 4% formaldehyde at 6 h postinfection and stained with polyclonal anti-P-Ser473-Akt-1 and Cy3. Images were taken at a magnification of ×40. (C) Modulations of Hsp/c70 protein level. HS indicates a positive control, showing the heat shock response of CV-1 cells that were placed at 55° for 1 h. Lamin B served as a loading control. (D) Confocal microscopy of Hsp/c70. Cells were fixed at the designated time points and stained with monoclonal anti-Hsp/c70 and Cy5. Photographs were taken at a magnification of ×60 with zoom 2.

induction has been previously observed in different cell types and organs (26). The regulating mechanism is not fully understood and may involve multiple factors. Confocal imaging (Fig. 4D) shows redistribution of Hsp/c70 between 6 and 9 h postinfection. While prior to that time Hsp/c70 is distributed throughout the cytoplasm, at 6 to 9 h it becomes perinuclear, with a patchy appearance.

The timing of Hsp/c70 upregulation and its cellular redistribution correlates with not only apoptotic arrest but also SV40 disassembly, consistent with the finding that chaperones participate in SV40 disassembly *in vitro* (17).

Cellular signaling induced by recombinant empty SV40 capsids. Large and small T antigens were previously reported to be involved in apoptotic processes as an inducer and suppressor, respectively (32). However, the time schedule of the signaling network studied here is not compatible with T-antigen activity since under our experimental conditions T antigens are detected only at 10 to 12 h postinfection (see Fig. S4A in the supplemental material), after genome entry to the nucleus that occurs at ~8 h (Kopatz and Oppenheim, unpublished). We considered the unlikely possibility that large T antigen, a nuclear protein, is assembled together with the minichromosome in SV40 virions and hitchhikes into the infected cells. However, this possibility was repeatedly rejected by a rigorous search for T antigen in mature virions (see Fig. S4B). If every virion particle contained just a single hexamer of T antigen, we would have expected ~500 ng of T antigen per 20 μg of total protein of purified full particles loaded in each lane. Thus, the signals studied here were not induced by T antigen.

As the signal is triggered soon after SV40 adsorption, before virus disassembly, we hypothesized that the major determinant is the viral external shell. Empty SV40 capsids are readily produced in *S. frugiperda* (Sf9) cells using recombinant baculovirus expressing VP1 from the polyhedrin promoter (50). VP1 spontaneously assembles in the nuclei of infected Sf9 cells, forming virus-like particles (VLPs). Purified VLPs appear as isolated nanoparticles, similar to wild-type SV40 virions (12). Gel electrophoresis experiments indicated that VLP preparations contain >95% VP1. Our experiments showed that infection of CV-1 cells with purified SV40 VLPs induced the same signaling cascade as infection with wild-type SV40. The data for Akt-1 activation, Hsp/c70 upregulation, and relocalization to the perinucleus have been previously published (12). Activation of PARP-1 and caspase-3, -6, and -10 and no activation of caspase-7 and -9 are presented in Fig. S5 in the supplemental material. The data obtained with VLPs are very similar to those for SV40 infection. These findings indicate that the signaling network studied here is triggered by the external shell alone and that there is no participation of any other viral protein, including T antigen.

SV40-infected cells do not proliferate in the absence of T antigen. We asked whether the induction of a signaling network triggered by SV40, including dramatic activation of Akt-1, leads to impaired cell cycle and/or proliferation of infected cells. To answer this question, we tested the effect of infection on the cell cycle by measuring DNA content by flow cytometry. As seen in Fig. 5A second row, and quantified in B, infection by wild-type SV40 leads to transition of the G_1-arrested cells (Fig. 5A, top row) to S phase at 24 h postinfection. This was expected, as SV40 T antigen was shown to stimulate host DNA replication, mostly by inactivation of p53 and retinoblastoma (Rb) (1, 23). Therefore, to establish whether there is cell proliferation via Akt-1, we have analyzed the effect of infection by constructs devoid of T antigen: (i) SV/*luc*, an SV40 derivative in which the gene for T antigen has been replaced by *luc* (the gene encoding luciferase); and (ii) SV40 VLPs that induce Akt-1 at levels equal to those of the wild-type virus even though they lack SV40 DNA (12). The results (Fig. 5) demonstrate that infection with VLPs or SV*luc* did not affect the host cell cycle. Thus, in spite the dramatic activation of Akt-1, infected cells do not proliferate in the absence of T antigen.

PLCγ, an inducer of the apoptotic, survival, and stress pathways. PARP-1 is commonly activated by DNA damage (30) and functions in DNA damage response. However, following SV40 infection, PARP-1 was already active at 1 h postinfection (Fig. 1A) while cellular DNA damage was not detected by the TUNEL assay at 9 to 24 h (Fig. 3). PARP-1 may also be activated by direct contact with the internal SV40 capsid protein VP3, as shown for the late phase of infection, leading to host cell necrosis and liberation of virion particles (27). But at 1 h postinfection, prior to disassembly, VP3 is still hidden inside the virion, which argues against this mechanism. Moreover, PARP-1 is a nuclear enzyme, which excludes direct contact with VP3 at that early time.

Activation of PARP-1 via inositol 1,4,5-triphosphate and Ca^{2+} mobilization, a signal downstream of PLCγ, was discovered in brain neuronal cells (29). We hypothesized that this mechanism may also function in the epithelium-derived cell line CV-1. In addition, activation of PLCγ via tyrosine phosphorylation in SV40-infected cells has been previously reported (43). We tested for PLCγ activation in SV40-infected cells by Western blotting with antibodies against phosphorylated PLCγ, followed by quantification of the bands. The results (Fig. 6A) demonstrate that activation starts within the first hour, with peaks at 2 and 6 h postinfection.

To test whether Akt-1 is activated by PLCγ, we analyzed extracts of infected cells treated with the PLCγ-specific inhibitor U73122. As in the other experiments, the cells were exposed to the inhibitor for 1 h prior to the infection. The extracts were analyzed by Western blotting for PARP-1. Lamin B, which does not change following infection (our unpublished results), was used as a loading control. The PARP-1 signals were quantified and normalized according to lamin B. The results of three independent experiments show that inhibition of PLCγ abrogates the activation of PARP-1 (Fig. 6B), indicating that the membrane signaling originally described for brain neurons (29) also operates in kidney epithelial cells.

Further experiments with the PLCγ inhibitor allowed us to place it in the signaling network. The results show that activation of Akt-1 (Fig. 6B) and upregulation of Hsp/c70 (Fig. 6B) are completely dependent on PLCγ activity. Upregulation of Hsp/c70 by PLCγ may occur via DAG, a second messenger synthesized by PLCγ which activates protein kinase C (PKC), a regulator of Hsp/c70 (19). The data points shown in Fig. 6B represent the averages of three experiments, normalized relative to values for mock-infected cells. The standard deviations indicate the high reproducibility of the results.

The role of PLCγ activation in SV40 infection was examined with the specific inhibitor U73122 added 1 h before virus ad-

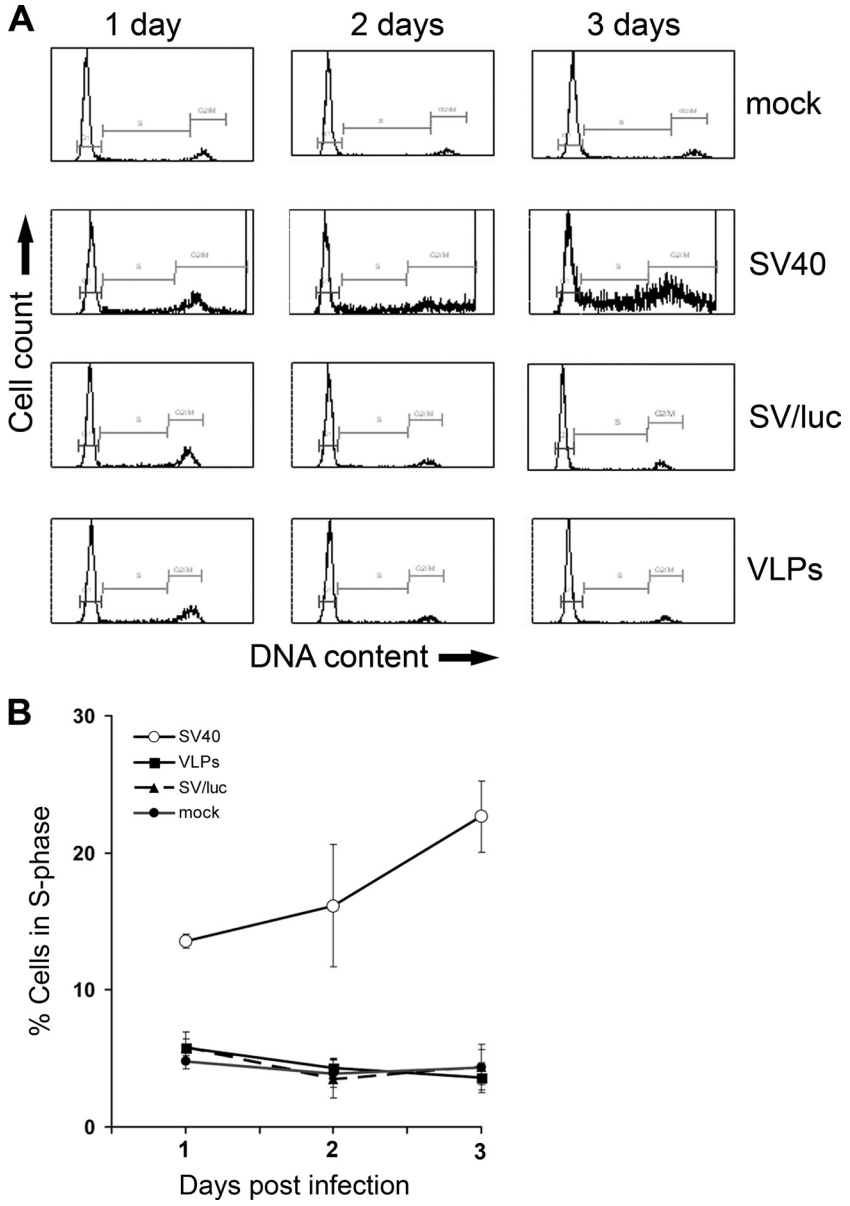

FIG. 5. Infected cells do not proliferate in the absence of T antigen. (A) Flow cytometry of cells infected with the constructs designated on the right. The cells were fixed in 100% ethanol, treated with RNase for 1 h, and analyzed by fluorescence-activated cell sorting (FACS) following staining with propidium iodide. (B) Graphical representation of S-phase cells; data are the average of three independent infection experiments.

sorption. As seen in Fig. 6C, the addition of the inhibitor completely abolished the infection process, as assayed by T-antigen expression, substantiating the role of PLCγ as an essential player in SV40-induced signaling. Control Western blotting for VP1 indicated that the cells that were negative for T antigen were infected with SV40 (see Fig. S3D in the supplemental material).

Akt-1 is known to be activated by PI3K. However, in our experiments Akt-1 activation was only partially reduced by inhibition of PI3K (Fig. 6B). The effect on T-antigen expression was minimal, suggesting that it was not required for the infection process. This may be due to incomplete inhibition of PI3K under our experimental conditions or to activation of Akt-1 independently of PI3K by an as yet unknown mechanism.

We concluded that PLCγ, which is most likely activated by SV40 binding to its cellular receptor GM1 (28, 59), is a major mediator of an SV40-induced signaling network.

DISCUSSION

The slow entry process of SV40 and mild effects on cellular metabolism allowed us to dissect previously unknown cross talk between signaling pathways. The present study demonstrates that the virus usurps a unique combination of cellular signals. The emerging preliminary network is summarized in Fig. 7. Pathways confirmed by inhibitor studies to be essential for productive SV40 infection are shown by heavy arrows.

While apoptosis is a common theme of host defense, viruses

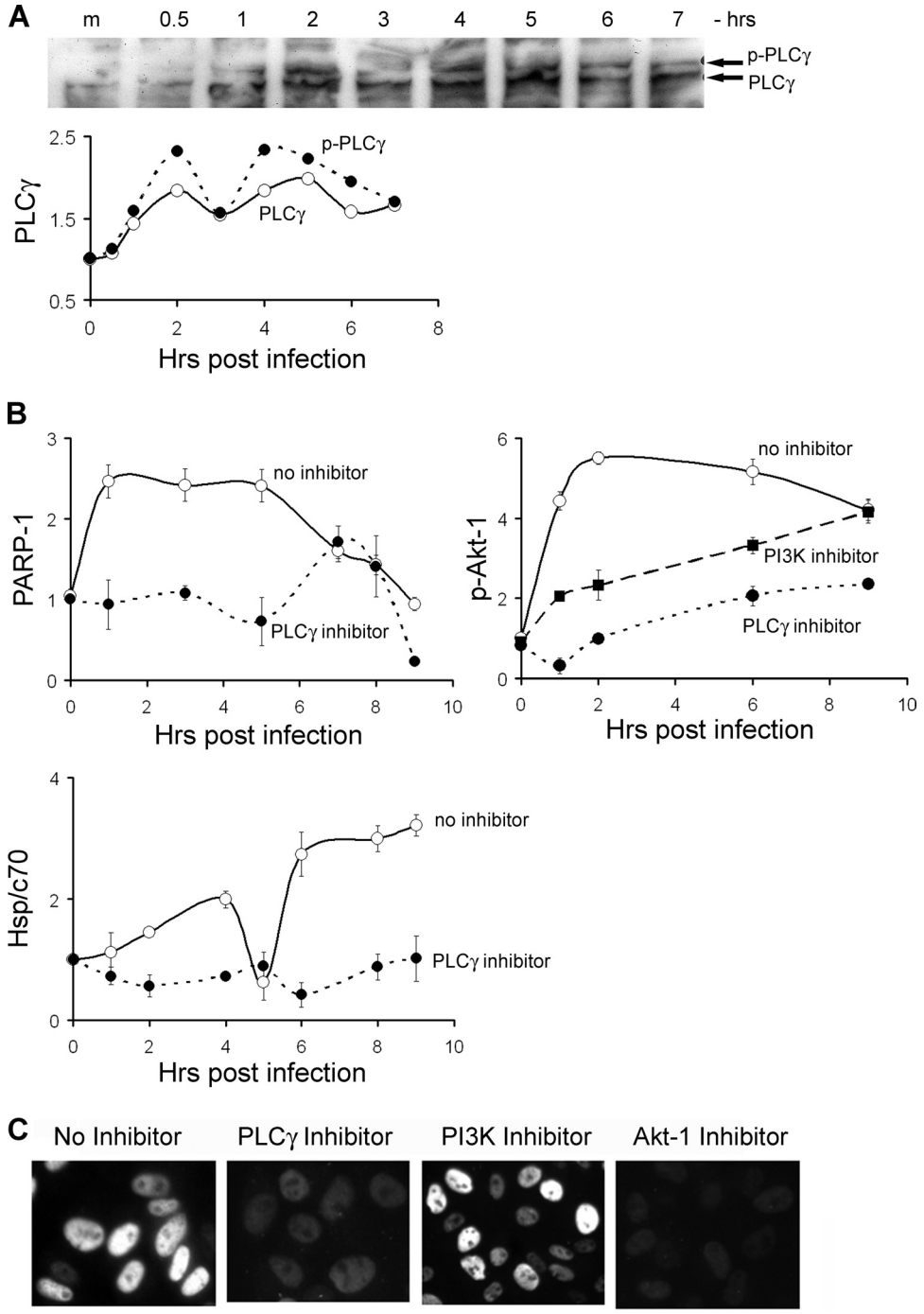

FIG. 6. PLCγ is a key element in SV40-induced signaling. (A) Activation of PLCγ, seen by appearance of the phosphorylated species. To clarify the bands, this image was auto level adjusted using Adobe Photoshop CS2. Quantification of PLCγ and its phosphorylated form is shown below. (B) Quantification of the levels of active PARP-1, P-Akt-1, and Hsp/c70 in the presence and absence of the PLCγ inhibitor U73122 (10 μM). The level of P-Akt-1 was also measured in the presence of PI3K inhibitor LY294002 (50 μM). The data points were normalized relative to lamin B, which served as a loading control. The average of three experiments with standard deviations are shown for each data point. (C) Expression of T antigen in infected cells in the presence of the following inhibitors: for PLCγ, 10 μM U73122; PI3K, 50 μM LY294002; Akt-1, 20 μM Tricibine V. All the inhibitors were added 1 h before adsorption. At these concentrations no cytotoxicity was observed during 3 days. Images were taken after 2 days.

use different strategies to counteract it. Those include manipulation of the DNA damage response (35), cell cycle regulation (61), and caspase inhibition (8). In contrast, SV40 hijacks PARP-1 and caspases to facilitate its infection process, as judged by lack of T-antigen expression in experiments with a PARP-1-negative cell line and caspase inhibitors. In addition, SV40 capsids trigger activation of the Akt-1 survival pathway exclusively for the purpose of arresting apoptosis without lead-

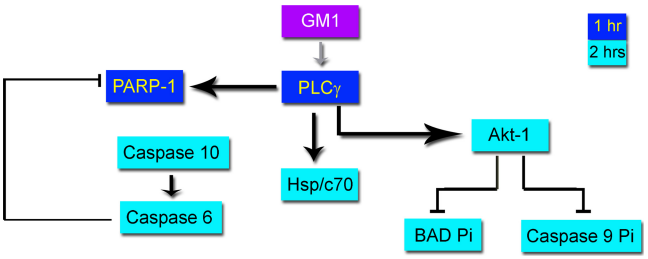

FIG. 7. SV40-triggered signaling network. Thick arrows designate pathways essential for productive SV40 infection, as confirmed by specific inhibitors. Thin arrows indicate known pathways, not confirmed in the present study. The role of GM1 in the activation of PLCγ is hypothetical.

ing to cellular proliferation. This also is in contrast to other viruses that activate the Akt-1 pathway as part of their respective tumorigenic processes. Thus, the SV40-triggered cellular signaling network is fundamentally distinct in more than one respect from the networks of other viruses.

Perhaps the most puzzling property of this network is that a single signaling protein, PLCγ, induces concurrently two counteracting pathways, apoptosis and survival. Remarkably, both PARP-1 and Akt-1 remain active during the same time frame, for 8 h, until nuclear entry is accomplished. During the whole period the cells neither undergo apoptosis nor proliferate, indicating a robust network that keeps the opposing pathways in a delicate balance. Furthermore, the intricate network appears to be activated by a single viral coat protein, VP1, presumably through its interaction with the GM1 receptor. Importantly, activation of PARP-1, Akt-1, and Hsp/c70, as well as lack of apoptosis and cell cycle arrest, is seen throughout the infected culture, indicating that these signals occur in each and every infected cell.

Our results show that caspases participate in SV40 infection although we have not found caspase cleavage consensus sequences in the capsid proteins; nor did we detect caspase cleavage products by Western blotting. The role of caspases in the infection is not yet clear. The pattern of caspase activation following SV40 infection is puzzling. While in many other cases caspase-8, -10, and -9 are activated at the initiation of apoptosis (15), here we see activation only of caspase-10. The consensus pathway for caspase-10 activation is via death receptors (47). As viruses are known to activate multiple receptors, it is possible that SV40 activates death receptors. Remarkably, in spite of the very low activation of caspase-6 and -10, their activity appears to be critical for the progress of the infection.

Our data strongly suggest that PARP-1 activation by PLCγ is mediated via Ca^{2+} signaling, as previously described for neuronal cells (29). Additional support is provided by our unpublished results, which have implicated the inositol triphosphate receptor (IP3R), the membrane glycoprotein complex acting as a Ca^{2+} channel, in SV40 entry. We found that the IP3R agonist oleol-L-α-lysophosphatidic acid (LPA) added at the first hour enhanced SV40 infection while 2-aminoethoxydiphenyl borate (2-APB), an IP3R antagonist, diminished the infection. To the best of our knowledge, this is the first description of activation of PARP-1 by PLCγ in nonneuronal cells, suggesting that this activation mechanism may have a wider occurrence than previously recognized.

Is there a role for T antigen in triggering the network described here? T antigen was shown to participate in apoptosis, cell cycle regulation, Akt-1 signaling, DNA damage response, and others cellular pathways (1, 60, 62). The present study focused on early virus-triggered signaling before T antigen is synthesized, which argues against its participation. Furthermore, we demonstrated that there is no T antigen in mature SV40 virion particles. Importantly, the signaling network presented in Fig. 7 was induced by both the wild-type virus and VLPs, which are composed exclusively of recombinant SV40 VP1. These findings prove that the network does not depend on T antigen.

The capacity of SV40 VLPs to induce the survival pathway and stress response may have medical implications for degenerative diseases. We have recently demonstrated that recombinant VLPs, devoid of DNA, significantly attenuate acute renal injury triggered in model animals by administration of nephrotoxic agents, including mercury (12) and *cis*-platinum (experiments in progress). We further showed that the underlying mechanisms involve induction of Hsp/c70 and the activation of Akt-1.

In conclusion, our study demonstrates that SV40 induces a novel signaling network that is fundamentally different from the networks described for other viruses so far. The virus activates PARP-1, presumably because it requires caspase activity for entry, by a mechanism still unknown; Akt-1 and perhaps also Hsp/c70 function in cell survival and apoptotic arrest, facilitating viral propagation; Hsp/c70 is most likely required for disassembly, together with other chaperones. Interestingly, SV40 elicits concurrent counteracting signaling of apoptosis and survival, leading neither to cell death nor to proliferation. The network presented here is triggered by a single protein, VP1, via a single mediator, PLCγ. The SV40-host interaction paradigm reflects the evolution of a delicate balance and fine-tuning between viral attack and host defense.

ACKNOWLEDGMENTS

This work was supported by the Israel Science Foundation (grant number 604/07) and U.S. Public Health Service grant CA100479.

We thank Itamar Simon and Robert Goldman for stimulating discussions and Gerald M. Cohen, Arieh Eden, Dvora Filon, and Orly Ben-nun-Shaul for critical reading of the manuscript. Mark Tarshish assisted in the confocal imaging. We are grateful to Z. Q. Wang for providing the $PARP^{-/-}$ and $PARP^{+/+}$ cells. Mahmoud Abd-El-Latif and Tameema Abdalla performed some of the experiments.

REFERENCES

1. **Ahuja, D., M. T. Saenz-Robles, and J. M. Pipas.** 2005. SV40 large T antigen targets multiple cellular pathways to elicit cellular transformation. Oncogene **24:**7729–7745.
2. **Al-Molawi, N., V. A. Beardmore, M. J. Carter, G. E. Kass, and L. O. Roberts.** 2003. Caspase-mediated cleavage of the feline calicivirus capsid protein. J. Gen. Virol. **84:**1237–1244.
3. **Anderson, H. A., Y. Chen, and L. C. Norkin.** 1998. MHC class I molecules are enriched in caveolae but do not enter with simian virus 40. J. Gen. Virol. **79:**1469–1477.
4. **Arya, R., M. Mallik, and S. C. Lakhotia.** 2007. Heat shock genes—integrating cell survival and death. J. Biosci. **32:**595–610.
5. **Ashkenazi, A.** 2002. Targeting death and decoy receptors of the tumour-necrosis factor superfamily. Nat. Rev. Cancer **2:**420–430.
6. **Basson, M. D.** 2008. An intracellular signal pathway that regulates cancer cell adhesion in response to extracellular forces. Cancer Res. **68:**2–4.
7. **Beere, H. M.** 2001. Stressed to death: regulation of apoptotic signaling pathways by the heat shock proteins. Sci. STKE **2001:**re1.
8. **Best, S. M.** 2008. Viral subversion of apoptotic enzymes: escape from death row. Annu. Rev. Microbiol. **62:**171–192.

9. **Bhattacharyya, S., H. E. Lorimer, and C. Prives.** 1995. Murine polyomavirus and simian virus 40 large T antigens produce different structural alterations in viral origin DNA. J. Virol. **69:**7579–7585.
10. **Black, P. H., E. M. Crawford, and L. V. Crawford.** 1964. The purification of simian virus 40. Virology **24:**381–387.
11. **Boatright, K. M., and G. S. Salvesen.** 2003. Mechanisms of caspase activation. Curr. Opin. Cell Biol. **15:**725–731.
12. **Butin-Israeli, V., D. Uzi, M. Abd-El-Latif, G. Pizov, A. Eden, Y. S. Haviv, and A. Oppenheim.** 2008. DNA-free recombinant SV40 capsids protect mice from acute renal failure by inducing stress response, survival pathway and apoptotic arrest. PLoS One **3:**e2998.
13. **Campanero-Rhodes, M. A., A. Smith, W. Chai, S. Sonnino, L. Mauri, R. A. Childs, Y. Zhang, H. Ewers, A. Helenius, A. Imberty, and T. Feizi.** 2007. *N*-Glycolyl GM1 ganglioside as a receptor for simian virus 40. J. Virol. **81:**12846–12858.
14. **Cantley, L. C.** 2002. The phosphoinositide 3-kinase pathway. Science **296:**1655–1657.
15. **Chen, M., and J. Wang.** 2002. Initiator caspases in apoptosis signaling pathways. Apoptosis **7:**313–319.
16. **Cheng, F., A. Y. Chen, S. M. Best, M. E. Bloom, D. Pintel, and J. Qiu.** 30 December 2009. The capsid proteins of Aleutian mink disease virus (AMDV) activate caspases and are specifically cleaved during infection. J. Virol. doi:10.1128/jvi.01917-09.
17. **Chromy, L. R., A. Oltman, P. A. Estes, and R. L. Garcea.** 2006. Chaperone-mediated in vitro disassembly of polyoma- and papillomaviruses. J. Virol. **80:**5086–5091.
18. **Dahl, J., J. You, and T. L. Benjamin.** 2005. Induction and utilization of an ATM signaling pathway by polyomavirus. J. Virol. **79:**13007–13017.
19. **Ding, X. Z., R. C. Smallridge, R. J. Galloway, and J. G. Kiang.** 1996. Increases in HSF1 translocation and synthesis in human epidermoid A-431 cells: role of protein kinase C and [Ca2+]. J. Invest. Med. **44:**144–153.
20. **Eash, S., W. Querbes, and W. J. Atwood.** 2004. Infection of Vero cells by BK virus is dependent on caveolae. J. Virol. **78:**11583–11590.
21. **Engelman, J. A., J. Luo, and L. C. Cantley.** 2006. The evolution of phosphatidylinositol 3-kinases as regulators of growth and metabolism. Nat. Rev. Genet **7:**606–619.
22. **Ewers, H., W. Römer, A. Smith, K. Bacia, S. Dmitrieff, W. Chai, R. Mancini, J. Kartenbeck, V. Chambon, L. Berland, A. Oppenheim, G. Schwarzmann, T. Feizi, P. Schwille, P. Sens, A. Helenius, and L. Johannes.** 2010. GM1 structure determines SV40-induced membrane invagination and infection. Nat. Cell Biol. **12:**11–18.
23. **Fanning, E.** 1992. Simian virus 40 large T antigen: the puzzle, the pieces, and the emerging picture. J. Virol. **66:**1289–1293.
24. **Fulda, S., and K. M. Debatin.** 2006. Extrinsic versus intrinsic apoptosis pathways in anticancer chemotherapy. Oncogene **25:**4798–4811.
25. **Galluzzi, L., C. Brenner, E. Morselli, Z. Touat, and K. G.** 2008. Viral control of mitochondrial apoptosis. PLoS Pathog. **4:**e1000018.
26. **Gonzalez, B., and R. Manso.** 2004. Induction, modification and accumulation of HSP70s in the rat liver after acute exercise: early and late responses. J. Physiol. **556:**369–385.
27. **Gordon-Shaag, A., Y. Yoseph, M. Abd-el-Latif, and A. Oppenheim.** 2003. The abundant nuclear enzyme PARP participates in the life cycle of SV40 and is stimulated by the virus minor capsid protein VP3. J. Virol. **77:**4273–4282.
28. **Gouy, H., P. Deterre, P. Debre, and G. Bismuth.** 1994. Cell calcium signaling via GM1 cell surface gangliosides in the human Jurkat T cell line. J. Immunol. **152:**3271–3281.
29. **Homburg, S., L. Visochek, N. Moran, F. Dantzer, E. Priel, E. Asculai, D. Schwartz, V. Rotter, N. Dekel, and M. Cohen-Armon.** 2000. A fast signal-induced activation of poly(ADP-ribose) polymerase: a novel downstream target of phospholipase C. J. Cell Biol. **150:**293–307.
30. **Kim, M. Y., T. Zhang, and W. L. Kraus.** 2005. Poly(ADP-ribosyl)ation by PARP-1: "PAR-laying" NAD+ into a nuclear signal. Genes Dev. **19:**1951–1967.
31. **Koh, D. W., T. M. Dawson, and V. L. Dawson.** 2005. Mediation of cell death by poly(ADP-ribose) polymerase-1. Pharmacol. Res. **52:**5–14.
32. **Kolzau, T., R. S. Hansen, D. Zahra, R. R. Reddel, and A. W. Braithwaite.** 1999. Inhibition of SV40 large T antigen induced apoptosis by small T antigen. Oncogene **18:**5598–5603.
33. **Kroemer, G., L. Galluzzi, P. Vandenabeele, J. Abrams, E. S. Alnemri, E. H. Baehrecke, M. V. Blagosklonny, W. S. El-Deiry, P. Golstein, D. R. Green, M. Hengartner, R. A. Knight, S. Kumar, S. A. Lipton, W. Malorni, G. Nunez, M. E. Peter, J. Tschopp, J. Yuan, M. Piacentini, B. Zhivotovsky, and G. Melino.** 2009. Classification of cell death: recommendations of the Nomenclature Committee on Cell Death 2009. Cell Death Differ. **16:**3–11.
34. **Lavrik, I. N., A. Golks, and P. H. Krammer.** 2005. Caspases: pharmacological manipulation of cell death. J. Clin. Invest. **115:**2665–2672.
35. **Lilley, C. E., R. A. Schwartz, and M. D. Weitzman.** 2007. Using or abusing: viruses and the cellular DNA damage response. Trends Microbiol. **15:**119–126.
36. **Manning, B. D., and L. C. Cantley.** 2007. AKT/PKB signaling: navigating downstream. Cell **129:**1261–1274.
37. **Marsh, M., and A. Helenius.** 2006. Virus entry: open sesame. Cell **124:**729–740.
38. **McStay, G. P., G. S. Salvesen, and D. R. Green.** 2008. Overlapping cleavage motif selectivity of caspases: implications for analysis of apoptotic pathways. Cell Death Differ. **15:**322–331.
39. **Neu, U., K. Woellner, G. Gauglitz, and T. Stehle.** 2008. Structural basis of GM1 ganglioside recognition by simian virus 40. Proc. Natl. Acad. Sci. U. S. A. **105:**5219–5224.
40. **Norkin, L. C., H. A. Anderson, S. A. Wolfrom, and A. Oppenheim.** 2002. Caveolar endocytosis of simian virus 40 is followed by brefeldin A-sensitive transport to the endoplasmic reticulum, where the virus disassembles. J. Virol. **76:**5156–5166.
41. **Park, S. J., C. H. Wu, J. D. Gordon, X. Zhong, A. Emami, and A. R. Safa.** 2004. Taxol induces caspase-10-dependent apoptosis. J. Biol. Chem. **279:**51057–51067.
42. **Parsons, J.** 2010. Phospholipase C gamma (PLC-gamma). Sci. Signal. http://stke.sciencemag.org/cgi/cm/stkecm;CMC_9055.
43. **Pelkmans, L., E. Fava, H. Grabner, M. Hannus, B. Habermann, E. Krausz, and M. Zerial.** 2005. Genome-wide analysis of human kinases in clathrin- and caveolae/raft-mediated endocytosis. Nature **436:**78–86.
44. **Pelkmans, L., D. Puntener, and A. Helenius.** 2002. Local actin polymerization and dynamin recruitment in SV40-induced internalization of caveolae. Science **296:**535–539.
45. **Polster, B. M., J. Pevsner, and J. M. Hardwick.** 2004. Viral Bcl-2 homologs and their role in virus replication and associated diseases. Biochim. Biophys. Acta **1644:**211–227.
46. **Richterova, Z., D. Liebl, M. Horak, Z. Palkova, J. Stokrova, P. Hozak, J. Korb, and J. Forstova.** 2001. Caveolae are involved in the trafficking of mouse polyomavirus virions and artificial VP1 pseudocapsids toward cell nuclei. J. Virol. **75:**10880–10891.
47. **Rieux-Laucat, F., A. Fischer, and F. L. Deist.** 2003. Cell-death signaling and human disease. Curr. Opin. Immunol. **15:**325–331.
48. **Rosenberg, B., J. Deutch, and G. Unger.** 1981. Growth and purification of SV40 virus for biochemical studies. J. Virol. Methods **3:**167–176.
49. **Saleh, A., S. M. Srinivasula, L. Balkir, P. D. Robbins, and E. S. Alnemri.** 2000. Negative regulation of the Apaf-1 apoptosome by Hsp70. Nat. Cell Biol. **2:**476–483.
50. **Sandalon, Z., and A. Oppenheim.** 1997. Self assembly and protein-protein interactions between the SV40 capsid proteins produced in insect cells. Virology **237:**414–421.
51. **Schelhaas, M., J. Malmstrom, L. Pelkmans, J. Haugstetter, L. Ellgaard, K. Grunewald, and A. Helenius.** 2007. Simian Virus 40 depends on ER protein folding and quality control factors for entry into host cells. Cell **131:**516–529.
52. **Shtilbans, V., M. Wu, and D. E. Burstein.** 2008. Current overview of the role of Akt in cancer studies via applied immunohistochemistry. Ann. Diagn. Pathol. **12:**153–160.
53. **Smith, A. E., and A. Helenius.** 2004. How viruses enter animal cells. Science **304:**237–242.
54. **Stang, E., J. Kartenbeck, and R. G. Parton.** 1997. Major histocompatibility complex class I molecules mediate association of SV40 with caveolae. Mol. Biol. Cell **8:**47–57.
55. **Stehle, T., S. J. Gamblin, Y. Yan, and S. C. Harrison.** 1996. The structure of simian virus 40 refined at 3.1 Å resolution. Structure **4:**165–182.
56. **Thorburn, A.** 2004. Death receptor-induced cell killing. Cell Signal. **16:**139–144.
57. **Tsai, B., J. M. Gilbert, T. Stehle, W. Lencer, T. L. Benjamin, and T. A. Rapoport.** 2003. Gangliosides are receptors for murine polyoma virus and SV40. EMBO J. **22:**4346–4355.
58. **Wang, Z. Q., B. Auer, L. Stingl, H. Berghammer, D. Haidacher, M. Schweiger, and E. F. Wagner.** 1995. Mice lacking ADPRT and poly(ADP-ribosyl)ation develop normally but are susceptible to skin disease. Genes Dev. **9:**509–520.
59. **Wu, G., Z. H. Lu, A. G. Obukhov, M. C. Nowycky, and R. W. Ledeen.** 2007. Induction of calcium influx through TRPC5 channels by cross-linking of GM1 ganglioside associated with α5β1 integrin initiates neurite outgrowth. J. Neurosci. **27:**7447–7458.
60. **Yu, Y., and J. C. Alwine.** 2008. Interaction between simian virus 40 large T antigen and insulin receptor substrate 1 is disrupted by the K1 mutation, resulting in the loss of large T antigen-mediated phosphorylation of Akt. J. Virol. **82:**4521–4526.
61. **Zhao, R. Y., and R. T. Elder.** 2005. Viral infections and cell cycle G2/M regulation. Cell Res. **15:**143–149.
62. **Zhao, X., R. J. Madden-Fuentes, B. X. Lou, J. M. Pipas, J. Gerhardt, C. J. Rigell, and E. Fanning.** 2008. Ataxia telangiectasia-mutated damage-signaling kinase- and proteasome-dependent destruction of Mre11-Rad50-Nbs1 subunits in simian virus 40-infected primate cells. J. Virol. **82:**5316–5328.
63. **Zhirnov, O. P., T. E. Konakova, W. Garten, and H. Klenk.** 1999. Caspase-dependent N-terminal cleavage of influenza virus nucleocapsid protein in infected cells. J. Virol. **73:**10158–10163.
64. **Zullo, J., C. D. Stiles, and R. L. Garcea.** 1987. Regulation of c-myc and c-fos mRNA levels by polyomavirus: distinct roles for the capsid protein VP1 and the viral early proteins. Proc. Natl. Acad. Sci. U. S. A. **84:**1210–1214.